JCTC Journal of Chemical Theory and Computation

Beyond the Wade−Mingos Rules in Bare 10- and 12-Vertex Germanium Clusters: Transition States for Symmetry Breaking Processes

R. B. King,*,† I. Silaghi-Dumitrescu,‡ and M. M. Uţă‡

Department of Chemistry, University of Georgia, Athens, Georgia, 30606, and Faculty of Chemistry and Chemical Engineering, Babeş-Bolyai University, Cluj-Napoca, Roumania

Received August 29, 2007

Abstract: The lowest energy structures of bare Ge_n^z clusters ($n = 10, 12$; $z = -6, 0, +2, +4$) obtained using density functional theory (DFT) at the hybrid B3LYP level often are relatively low-symmetry polyhedra not readily recognizable by the Wade−Mingos rules. However, such optimized structures may arise from higher symmetry transition states through symmetry breaking processes. Thus the lowest energy structures for the Ge_{10}^{6-} and Ge_{12}^{6-} clusters with hyperelectronic *arachno* $2n + 6$ skeletal electron counts are derived from pentagonal and hexagonal prism transition states, respectively, and retain the pentagonal and hexagonal faces of the prisms upon symmetry-breaking optimization. In addition, a variety of capped cube, prism, and antiprism transition states are found for the hypoelectronic Ge_{10}^{4+}, Ge_{12}, and Ge_{12}^{4+} clusters, which go to low-energy low-symmetry optimized structures, typically C_s or C_i, upon following the normal modes of the imaginary vibrational frequencies.

1. Introduction

The Wade−Mingos rules[1−4] historically were derived in order to relate the structures of polyhedral boranes and isoelectronic compounds to the number of skeletal electrons.[5] However, they subsequently have been used to explain the shapes of other cluster structures isoelectronic and isolobal with boranes. According to the Wade−Mingos rules the polyhedra in the so-called *closo* boranes $B_nH_n^{2-}$ and isoelectronic compounds with $2n + 2$ skeletal electrons are the most spherical deltahedra, namely polyhedra in which all faces are triangles and the vertices are as similar as possible. These deltahedral boranes can be considered to be three-dimensional aromatic systems[6,7] with $2n$ of the $2n + 2$ skeletal electrons being used for surface bonding analogous to the σ-bonding in benzene. The remaining two skeletal electrons are used for an n-center two-electron core bond involving overlap of inward pointing radial orbitals from each of the n vertex atoms at the center of the deltahedron. This latter bond in the deltahedral boranes plays an analogous role to the π-bonding in benzene. For the 10- and 12-vertex structures of interest in this paper the most spherical deltahedra found in the *closo* boranes $B_{10}H_{10}^{2-}$ and $B_{12}H_{12}^{2-}$ and related compounds are the D_{4d} bicapped square antiprism and the I_h regular icosahedron, respectively (Figure 1). Note that in counting skeletal electrons in the clusters of interest in this paper either a BH or bare Ge vertex is a donor of two skeletal electrons.

Now consider hyperelectronic (electron-rich) polyhedral boranes having more than $2n + 2$ skeletal electrons. The so-called *nido* boranes with n vertices have $2n + 4$ skeletal electrons and polyhedral structures with one nontriangular face. Frequently such *nido* borane structures can be derived from a *closo* borane structure with $n + 1$ vertices by removing one vertex and its associated edges. Thus the 10-vertex *nido* borane polyhedron, found in the long-known relatively stable[8] $B_{10}H_{14}$, can be obtained by removal of the unique degree 6 vertex from the 11-vertex *closo* deltahedron (Figure 2). Similarly the 12-vertex *nido* borane polyhedron, found in the ligand[9] $C_2B_{10}H_{12}^{2-}$ obtained by reduction of the carborane $C_2B_{10}H_{12}$, can be formally obtained by removal

* Corresponding author e-mail: rbking@chem.uga.edu.
† University of Georgia.
‡ Babeş-Bolyai University.

10.1021/ct7002226 CCC: $40.75
Published on Web 12/15/2007

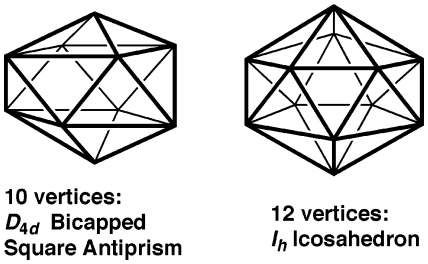

Figure 1. The most spherical (*closo*) deltahedra with 10 and 12 vertices.

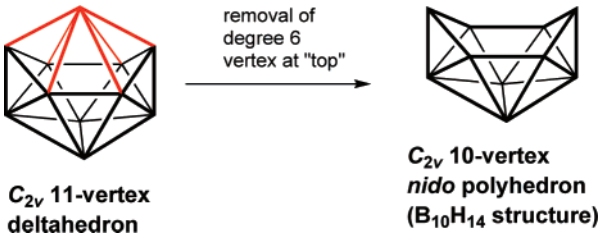

Figure 2. Conversion of the 11-vertex most spherical deltahedron to the 10-vertex *nido* polyhedron (found in $B_{10}H_{14}$) by removal of the unique degree 6 vertex (the "top" vertex) and the associated edges (colored red).

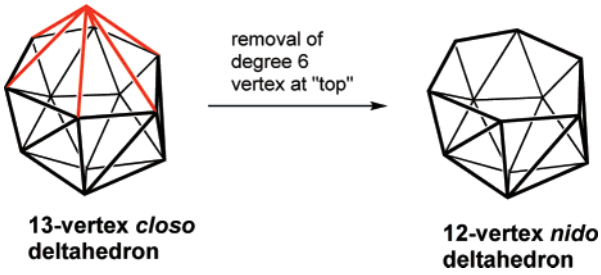

Figure 3. Conversion of the 13-vertex most spherical deltahedron to the 12-vertex *nido* polyhedron (found in the $C_2B_{10}H_{12}^{2-}$ ligand in $(\eta^5\text{-}C_5H_5)CoC_2B_{10}H_{12}$) by removal of the unique degree 6 vertex (the "top" vertex) and the associated edges (colored red).

of a degree 6 vertex from the 13-vertex *closo* polyhedron found in metallaboranes such as $(\eta^5\text{-}C_5H_5)CoC_2B_{10}H_{12}$ (Figure 3).

The Wade−Mingos rules in borane chemistry have been extended to systems even more hyperelectronic than the *nido* compounds such as the *arachno* compounds with $2n + 6$ skeletal electrons and two nontriangular faces or one large nontriangular face and the *hypho* compounds with $2n + 8$ skeletal electrons and an even more open structure. In principle, the *arachno* and *hypho* structures with n vertices can be derived from *closo* structures with $n + 2$ or $n + 3$ vertices, respectively, by removal of two or three vertices, respectively. However, as the structures become electron-richer the increasingly open polyhedra become increasingly less recognizable.

The Wade−Mingos rules[1−4] are more difficult to apply to hypoelectronic (electron-poor) clusters containing fewer than the $2n + 2$ skeletal electrons of *closo* structures. Such systems are not found in borane and carborane derivatives containing exclusively boron and carbon vertices so that they were not considered in Wade's original work.[1,2] However, hypoelectronic structures are found in isoelectronic metal carbonyl clusters and bare post-transition element clusters. Hypoelectronic structure types found in systems with n vertices and less than $2n + 2$ skeletal electrons include the following: (1) a capped deltahedron with $m < n$ vertices, typically for a system with $m + 2$ skeletal electrons such as the capped octahedral osmium carbonyl cluster[10] $Os_7(CO)_{21}$ ($v = 7$ but $m = 6 \Rightarrow 14$ skeletal electrons) and (2) "flattened" deltahedra with f "flattened" vertices pushed toward the center of the deltahedron,[11] typically for a system with $v - f + 2$ skeletal electrons such as the In_{11}^{7-} cluster found in K_8In_{11} ($v = 11$, $f = 3 \Rightarrow 18$ skeletal electrons).[12]

In recent years the chemistry of bare post-transition-metal clusters has expanded greatly from the original work of Zintl and co-workers.[13−16] Such clusters can be considered to be formally isoelectronic with boranes and carboranes.[17] Thus a bare group 14 element vertex (Si, Ge, Sn, Pb) is a donor of two skeletal electrons like a B−H vertex in boranes. Similarly a bare group 15 element vertex (P, As, Sb, Bi) is a donor of three skeletal electrons like a C−H vertex in carboranes. However, in many cases the polyhedra found in bare post-transition-metal clusters are different from those found in boranes and related compounds. Furthermore, they do not relate obviously to polyhedra suggested by the Wade−Mingos rules,[1−4] particularly in the cases of electron-poor clusters containing bare group 13 elements (Al, Ga, In, Tl), which are donors of only one skeletal electron. In order to understand such unusual polyhedra and the chemical bonding in such structures we have performed density functional theory (DFT) studies of germanium clusters containing from 5 to 12 germanium atoms.[18−23] Germanium was chosen as a model vertex atom to minimize the charges on clusters isoelectronic with the known molecules of interest.

Our studies as well as the work of others have indicated major differences between isoelectronic boranes and carboranes, on the one hand, and bare germanium and other post-transition-metal clusters, on the other hand. Examples are the following: (1) The antiaromaticity of the icosahedral E_{12}^{2-} (E = Si, Ge) as compared with the strong aromaticity of the isoelectronic $B_{12}H_{12}^{2-}$ as noted above.[24,25] (2) The lowest energy structure for Ge_{11}^{2-} is not the most spherical 11-vertex deltahedron[22] found in the stable borane $B_{11}H_{11}^{2-}$. (3) The lowest energy structure for Ge_8^{2-} is the spherically aromatic T_d tetracapped tetrahedron rather than the bisdisphenoid found in $B_8H_8^{2-}$ and related compounds.[19] These differences between isoelectronic bare germanium and borane clusters appear to be a consequence of the fact that the external germanium lone pair electrons can participate in the skeletal bonding, whereas no comparable electrons are available from the B−H vertices of boranes.

We have also observed many low-energy low-symmetry (not readily recognizable) germanium clusters Ge_n^z, particularly those with fewer than $2n + 2$ skeletal electrons. Such polyhedra often arise during the optimization of more obvious symmetrical polyhedra by following imaginary vibrational frequencies. The more symmetrical and thus more recognizable polyhedra can then be considered as transition states linking isomeric polyhedra of low symmetry. Thus a useful way of characterizing unsymmetrical low-energy

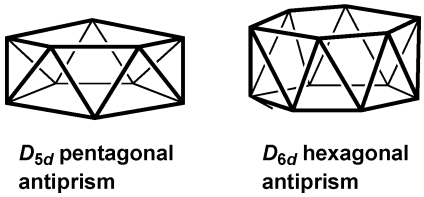

Figure 4. The pentagonal and hexagonal antiprisms as possible *arachno* polyhedra with two nontriangular faces (namely pentagons and hexagons, respectively).

polyhedra is by the more symmetrical transition states from which they arise.

A previous paper from our group[26] considers low-energy low-symmetry structures of hypoelectronic 11-vertex bare germanium clusters Ge_{11}^{z}. In that case, consideration of transition states leading to such clusters is less useful since relatively few chemically relevant 11-vertex polyhedra are readily recognizable because of their generally low symmetries. The present paper discusses the transition states leading to the low-energy low-symmetry structures of 10- and 12-vertex bare germanium clusters Ge_{10}^{z} $z = +4$ and Ge_{12}^{z} $z = 0, +4$ found in our previous work.[21,23] In this case, the low-symmetry structures often arise from readily recognizable symmetrical transition states. This paper characterizes such transition states, both for hypoelectronic Ge_{10}^{z} and Ge_{12}^{z} clusters as well as for hyperelectronic Ge_{10}^{6-} and Ge_{12}^{6-} clusters. The Ge_{10}^{6-} and Ge_{12}^{6-} clusters with the $2n + 6$ *arachno* skeletal electron counts are of interest since the readily recognizable pentagonal and hexagonal antiprism structures satisfying the *arachno* requirement of $2n + 6$ skeletal electrons and two obvious nontriangular faces (Figure 4) are not the lowest energy structures.

2. Theoretical Methods

The density functional theory (DFT) methods used in this paper are described in our previous papers on Ge_{10}^{z} and Ge_{12}^{z} clusters.[21,23] Thus the geometry optimizations were carried out at the hybrid DFT B3LYP level[27−30] with the 6-31G(d) (valence) double-ζ quality basis functions extended by adding one set of polarization (d) functions. The Gaussian 98 package of programs[31] was used in which the fine grid (75, 302) is the default for numerically evaluating the integrals and the tight (10^{-8}) hartree stands as default for the self-consistent field convergence. The symmetries were maintained during the initial geometry optimization processes. In the systems of interest in this paper the transition states of interest were optimized structures with significant imaginary vibrational frequencies, typically above $100i$ cm^{-1}. Symmetry breaking using the normal modes of these transition states defined by these imaginary vibrational frequencies was then used to determine optimized structures with minimum energies. Both the transition states and the final optimized structures are discussed in this paper with their relationships being depicted in Figures 5−11 (and Figures 1S−6S in the Supporting Information) with the energy differences between the transition state and the final structure approximately according to scale.

One might raise the legitimate question if this method is suitable for describing subtle electronic effects governing the structure of germanium clusters. In this connection Archibong and St. Amant[32] have shown that CCSD(T) calculations on Ge_6^{z} ($z = 0, -1$) give similar results to those obtained at the B3LYP DFT level of theory.

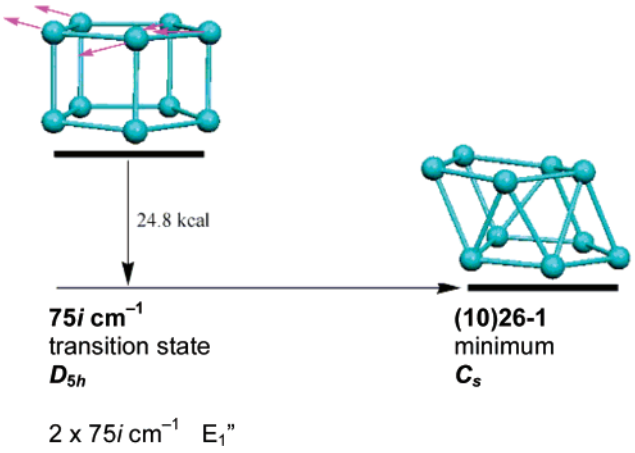

Figure 5. The distortion of the pentagonal prism transition state in Ge_{10}^{6-} along the E_1 normal mode of the $75i$ cm^{-1} vibrational frequency to give the global minimum **(10)26-1**.

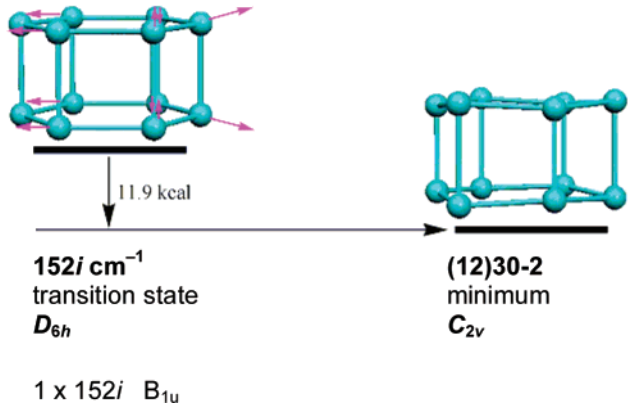

Figure 6. The distortion of the hexagonal prism transition state in Ge_{12}^{6-} along the B_{1u} normal mode of the $152i$ cm^{-1} vibrational frequency to give the lowest energy polyhedral structure **(12)30-2**.

The individual structures are labeled according to the number of skeletal electrons and relative energies with the specific relative energy designations matching those in the previous papers.[21,23] In addition, structures with 10 and 12 vertices are distinguished by the designations (10) and (12), respectively, in front of their structure labels. Thus the lowest energy structure of the 10-vertex 26 skeletal electron system Ge_{10}^{6-}, designated as **26-1** in the previous paper,[21] is now designated as **(10)26-1** (see Figure 5) in order to differentiate it from the lowest energy 12-vertex structure with 26 skeletal electrons, which would now be designated as **(12)26-1**.

3. Results

3.1. The Systems Ge_{10}^{6-} and Ge_{12}^{6-} with the *arachno* $2n + 6$ Skeletal Electron Counts. The Wade−Mingos rules[1−4] suggest that the D_{5d} pentagonal antiprism (Figure 4) should be the global minimum for the 26 ($=2n + 6$ for $n = 10$) skeletal electron 10-vertex system Ge_{10}^{6-} with an *arachno* skeletal electron count. Indeed a pentagonal antiprismatic

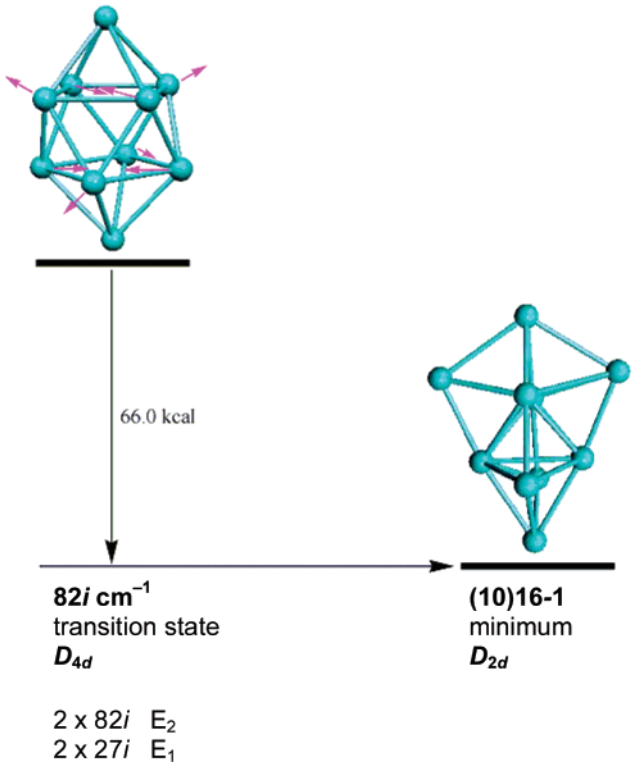

Figure 7. The distortion of the D_{4d} bicapped square antiprism transition state in Ge_{10}^{4+} along the E_2 normal mode of the 82*i* cm^{-1} vibrational frequency to give the lowest energy polyhedral structure **(10)16-1**.

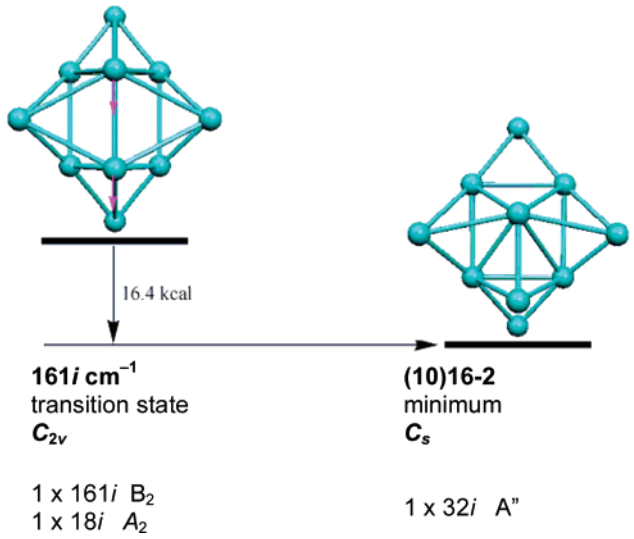

Figure 8. The distortion of the C_{2v} tetracapped trigonal prism transition state in Ge_{10}^{4+} along the B_2 normal mode of the 161*i* vibrational frequency to give the C_s polyhedral structure **(10)16-2**.

structure **(10)26-3** is found for Ge_{10}^{6-} but at 17.1 kcal/mol above the global minimum[21] **(10)26-3**. Optimization of a D_{5h} pentagonal prism starting structure leads to a pentagonal prismatic transition state with a 75*i* cm^{-1} imaginary vibrational mode. Following the corresponding E_1'' normal mode lowers the energy of the structure by 24.8 kcal/mol leading to the global minimum **(10)26-1** observed[21] for Ge_{10}^{6-} (Figure 5). The polyhedron in **(10)26-1** is derived from a D_{5h} pentagonal prism by distortion of the top pentagonal face

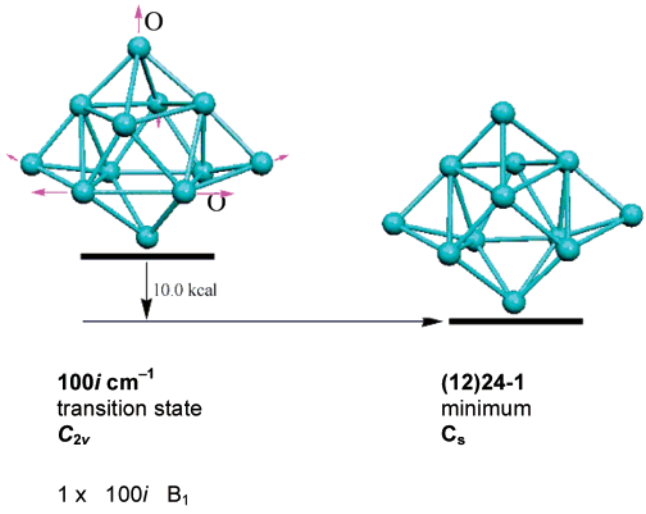

Figure 9. The distortion of the C_{2v} tetracapped square antiprism transition state in Ge_{12} along the normal mode of the 100*i* B_1 vibrational frequency to give the C_s polyhedral structure **(12)24-1**.

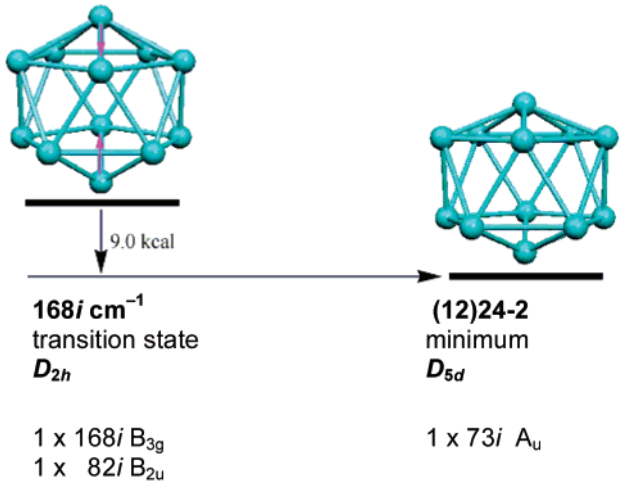

Figure 10. The distortion of the D_{2h} irregular icosahedron transition state in Ge_{12} along the B_{2g} normal mode of the 168*i* vibrational frequency to give the D_{5d} bicapped pentagonal antiprismatic structure **(12)24-2**.

relative to the bottom face so that the five rectangular faces linking the two pentagonal faces in the original prism become two rectangular and six triangular faces by the addition of diagonals across three of the original rectangular faces. This distortion necessarily destroys the original C_5 axis in the pentagonal prism. Also note that the **(10)26-1** polyhedron is intermediate between the pentagonal prism with five rectangular faces between the two pentagonal faces and the pentagonal antiprism with ten triangular faces between the two pentagonal faces.

The Wade−Mingos rules[1−4] also suggest that the D_{6d} hexagonal antiprism (Figure 4) should be the global minimum for the 30 ($=2n + 6$ for $n = 12$) skeletal electron 12-vertex system Ge_{12}^{6-} with the *arachno* skeletal electron count. Indeed a hexagonal antiprismatic structure **(12)30-5** is found for Ge_{12}^{6-} but at 23.1 kcal/mol above the lowest energy polyhedral structure **(12)30-2**.[23] Optimization of the D_{6h} hexagonal prism leads to a hexagonal prismatic transition

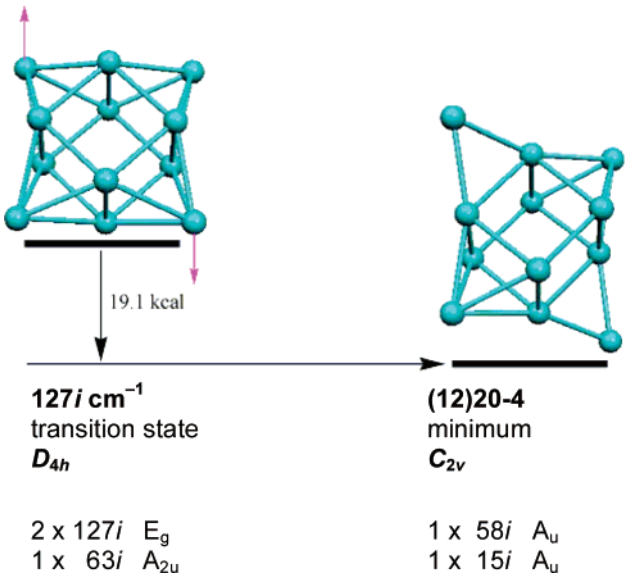

Figure 11. The distortion of the D_{4h} tetracapped cube transition state in Ge_{12}^{4+} along the E_g normal mode of the 127*i* vibrational frequency to give the C_{2v} structure **(12)20-4**.

state with a 152*i* cm^{-1} imaginary vibrational mode. Following the corresponding B_1 normal mode lowers the energy of the structure by 11.9 kcal/mol leading to the lowest energy polyhedral structure **(12)30-2** calculated for Ge_{10}^{6-} (Figure 6). This structure retains the topology of the hexagonal prism (i.e., the two hexagonal faces and the six quadrilateral faces between the two hexagonal faces) but destroys the C_6 axis.

3.2. The Hypoelectronic Cluster Ge_{10}^{4+}. The global minimum **(10)16-1** for Ge_{10}^{4+} with 16 skeletal electrons is derived from a relatively high energy D_{4d} bicapped square antiprism transition state (Figure 7). Following the E_2 normal mode corresponding to the largest imaginary vibrational frequency (82*i*) reduces the energy of the system by a gigantic 66.0 kcal/mol. The symmetry is concurrently reduced from D_{4d} to D_{2d} leading to a polyhedron derived from two interlocking planar pentagons at right angles to each other, which resembles a "Siamese twin" of two pentagonal bipyramids (Figure 7). Note that the pentagonal bipyramid building block of structure **(10)16-1** is the most spherical deltahedron with seven vertices and thus requires $2n + 2 = 16$ skeletal electrons for $n = 7$ by the Wade−Mingos rules.[1−4]

The next higher energy structure **(10)16-2** for Ge_{10}^{4+}, at 14.5 kcal/mol above **(10)16-1** discussed above, is derived from a C_{2v} tetracapped trigonal prism transition state (Figure 8). Following the B_2 normal mode of the largest imaginary frequency (161*i*) adds diagonals across two rectangular faces of the underlying trigonal prism with concurrent conversion of the corresponding two rectangular face caps to triangular face caps. The symmetry is thus reduced from C_{2v} to C_s and the energy by 16.4 kcal/mol (Figure 8). A relatively small imaginary vibrational frequency of 32*i* remains in **(10)16-2**, which might arise from a numerical integration error.[33,34]

A C_{2v} bicapped cube is the transition state to a C_s higher energy structure **(10)16-4** for Ge_{10}^{4+} (Figure 1S), which lies 20.6 kcal/mol above the global minimum **(10)16-1** (Figure 7). Following the B_1 normal mode corresponding to the relatively large 342*i* imaginary vibrational frequency in the bicapped cube reduces the symmetry from C_{2v} to C_s. However, the energy is reduced by only 7.9 kcal/mol with no significant change in the polyhedron topology.

3.3. The Neutral 12-Vertex Cluster Ge_{12}. The lowest energy structures for the neutral Ge_{12} cluster with 24 skeletal electrons are relatively low-symmetry structures derived by distortion of higher energy transition states. The global minimum for Ge_{12}, namely **(12)24-1** (Figure 9), is derived from a C_{2v} tetracapped square antiprism transition state by distortion along the B_1 normal mode corresponding to the 100*i* cm^{-1} vibrational frequency. The symmetry is reduced from C_{2v} to C_s, and two pairs of triangular faces in the original tetracapped square antiprism are opened (following the arrows marked by "O" in Figure 9) up into two quadrilateral faces. Removal of the two vertices capping triangular faces from the **(12)24-1** polyhedron leaves a 10-vertex polyhedron with 14 triangular faces and one quadrilateral face. This is a 10-vertex *nido* polyhedron and thus expected by the Wade−Mingos rules[1−4] to have the $2n + 4 = 24$ for $n = 10$ skeletal electrons found in Ge_{12}.

The next higher energy structure **(12)24-2** for Ge_{12}, at 21.9 kcal/mol above **(12)24-1** discussed above, is derived from an irregular D_{2h} icosahedron transition state by distortion along the B_{3g} normal mode corresponding to the largest imaginary frequency at 168*i* cm^{-1} (Figure 10). This normal mode involves compression of a pair of antipodal vertices and leads to a compressed (oblate) bicapped pentagonal antiprism still retaining the topology of the original icosahedron (i.e., no edges are broken). This process lowers the energy by 9.0 kcal/mol (Figure 10).

The next higher energy structure **(12)24-3** for Ge_{12}, at 23.5 kcal/mol above **(12)24-1** discussed above, is derived from a D_{6d} hexagonal antiprism transition state by distortion along the E_4 normal mode corresponding to the largest imaginary frequency at 143*i* cm^{-1} (Figure 2S). This process lowers the energy by a very large 58.9 kcal/mol and the symmetry from D_{6d} to D_{2d}. Each of the hexagonal faces of the original hexagonal antiprism becomes a pair of trapezoidal faces by formation of new transannular edges.

A higher energy structure for Ge_{12}, namely **(12)24-6** at 28.2 kcal/mol above the global minimum **(12)24-1**, is obtained from a D_{4h} tetracapped cube by distortion along the E_g normal mode corresponding to the 114*i* cm^{-1} vibrational frequency (Figure 3S). The process lowers the energy by 12.8 kcal/mol and the symmetry from D_{4h} to C_{2v}. The polyhedron in the resulting structure **(12)24-6** can be described as a pair of C_{2v} bicapped trigonal prisms sharing their uncapped rectangular faces.

3.4. The Lowest Energy Structure of Ge_{12}^{2+}. The lowest energy structure for Ge_{12}^{2+}, namely the D_{3d} hexacapped octahedron **(12)22-1**, is derived from a D_{4h} tetracapped cube transition state (Figure 4S) by a distortion along the E_g normal mode corresponding to the 95*i* cm^{-1} vibrational frequency. This process replaces the original 4-fold axis with a 3-fold axis and lowers the energy by 42.8 kcal/mol. Since the D_{3d} point group of the hexacapped octahedron is obviously not a subgroup of the D_{4h} point group of the

Table 1. Seven Transition States within 25 kcal/mol of the Final Optimized Structures

figure	species	transition state	imaginary frequencies[a]	symmetry breaking[c]	energy gain[b]/ binding energy/atom[d] (transition state/minimum)
			Hyperelectronic (*arachno*) Species		
5	Ge_{10}^{6-}	pentagonal prism	$75i(E_1'')$	$D_{5h}\rightarrow C_s$	24.8/+8.1/5.6
6	Ge_{12}^{6-}	hexagonal prism	$152i(B_{1u})$	$D_{6h}\rightarrow C_{2v}$	11.9/−19.9/−20.9
			Hypoelectronic Species		
8	Ge_{10}^{4+}	tetracapped trigonal prism	$161i(B_2),18i(A_2)$	$C_{2v}\rightarrow C_s$	16.4/−55.9/−57.5
S1	Ge_{10}^{4+}	bicapped cube	$342i(B_1),48i(B_2)$	$C_{2v}\rightarrow C_s$	7.9/−56.1/−56.9
9	Ge_{12}	tetracapped square antiprism	$100i(B_1)$	$C_{2v}\rightarrow C_s$	10.0/−112.2/−113.0
10	Ge_{12}	irregular icosahedron (D_{2h})	$168i(B_{3g}),82i$	$D_{2h}\rightarrow D_{5d}(73i)$[c]	9.0/−110.4/−111.2
11	Ge_{12}^{4+}	tetracapped cube	$127i(E_g),62i(A_{2u})$	$D_{4h}\rightarrow C_{2v}(58i)$	19.1/−69.8/−71.4

[a] Residual imaginary vibrational frequencies are given in parentheses. [b] Difference between the energy of the transition state and that of the optimized structure (kcal/mol). [c] This represents a symmetry change rather than symmetry breaking. [d] Difference between the energy of the cluster and the sum of the energies of the components divided by the number of atoms (kcal/mol).

tetracapped cube transition state, this is not a simple symmetry breaking process.

3.5. Several Structures for Ge_{12}^{4+}. The global minimum for Ge_{12}^{4+}, namely **(12)20-1**, is a C_{2v} structure that does not resemble anything actually found in a chemical system.[23] The next highest energy structure for Ge_{12}^{4+}, namely **(12)-20-2** at 8.0 kcal/mol above the global minimum **(12)20-1**, is a D_{4h} double cube, which can be derived from an O_h cuboctahedron transition state by distortion along the E_u normal mode of the highest imaginary vibration, namely the $417i$ cm^{-1} frequency (Figure 5S). This process is a drastic rearrangement that lowers the energy of the system by a gigantic 164.4 kcal/mol.

The next higher energy structure for Ge_{12}^{4+}, namely **(12)-20-3** at 8.9 kcal/mol above **(12)20-1**, is derived from a D_{4h} double square antiprism transition state. Following the E_g normal mode corresponding to the highest imaginary vibrational frequency, namely the $123i$ cm^{-1} frequency, lowers the energy by a large 62.0 kcal/mol and the symmetry from D_{4h} to C_i to give a much more open structure than the original double square antiprism (Figure 5S).

The next structure for Ge_{12}^{4+}, namely the C_{2v} structure (**12**)**20-4** at 10.5 kcal/mol above the global minimum **(12)-20-1**, is derived from a D_{4h} tetracapped cube transition state (Figure 11). Distortion along the E_g normal mode of the largest imaginary frequency at $127i$ reduces the symmetry from D_{4h} to C_{2v} with two opposite face caps becoming edge caps. This process results in an energy gain of 19.1 kcal/mol.

4. Discussion

The figures in the text and the Supporting Information depict 12 transition states leading to previously obtained[21,23] optimized structures for Ge_n^{6-} ($n = 10, 12$), Ge_{10}^{4+}, Ge_{12}, Ge_{12}^{2+}, and Ge_{12}^{4+} including global minima. The polyhedra in most of these optimized low-energy structures are not readily recognizable by the Wade−Mingos rules.[1−4] Of these 12 transition states, seven of them (Table 1) are within 25 kcal/mol of the optimized structure and thus are potentially chemically significant. The remaining five higher energy transition states, at energies ranging from 42.8 to 164.4 kcal/mol above the corresponding optimized structure, are significant mainly in indicating the route used for the DFT optimizations. These are the closest ones to the final optimized structures of any of the initial structures investigated. This is particularly true for the D_{4h} tetracapped cube transition state leading to the D_{3d} hexacapped octahedron global minimum **(12)22-1** of Ge_{12}^{4+} (Figure S3), since D_{3d} is not a subgroup of D_{4h} so that the conversion of the tetracapped cube to a hexacapped octahedron is not a simple symmetry breaking process.

A true transition state exhibits exactly one significant imaginary vibrational frequency, the normal mode of which indicates the pathway to the corresponding minimum point. Additional small imaginary frequencies significantly below $100i$ cm^{-1} can be attributed to errors arising from the numerical integration procedure.[33,34] The seven transition states listed in Table 1 all have exactly one imaginary vibrational frequency at or above $100i$ cm^{-1} except for the pentagonal prism transition state for Ge_{10}^{6-} (Figure 5), which has a single imaginary vibrational frequency at $75i$ cm^{-1}, which was followed in the optimization to the global minimum **(10)26-1** for Ge_{10}^{6-}. Two of the optimized structures in Table 1, namely the D_{5d} bicapped pentagonal antiprism structure **(12)24-2** for Ge_{12}, derived from a D_{2h} irregular icosahedron transition state (Figure 11), and the C_{2v} structure **(12)20-4** for Ge_{12}^{4+}, derived from a D_{4h} tetracapped cube transition state (Figure 11), have residual imaginary vibrational frequencies below $100i$ cm^{-1} after optimization. These structures are low-energy structures for Ge_{12} and Ge_{12}^{4+}, respectively, but are not their global minima.

Most of the high-energy transition states correspond to structures that are relatively far removed from the final structure and have more than one imaginary vibrational frequency large enough to be significant, thereby corresponding more accurately to higher order saddle points. The most extreme case of this type found in this work is the cuboctahedron for Ge_{12}^{4+}, which has three imaginary vibrational frequencies above 100 cm^{-1}, namely $417i$ cm^{-1} (E_u), $290i$ cm^{-1} (T_{2u}), and $115i$ (T_{1g}) as well as smaller imaginary vibrational frequencies at $36i$ (A_{2g}) and $29i$ (E_g). Following the normal mode corresponding to the $417i$ cm^{-1} vibrational frequency results in the gigantic energy lowering of 164.4 kcal/mol and a rather drastic rearrangement leading to a D_{4h} double cube stationary point **(12)20-2**. This corresponds to the lowest energy chemically realistic structure[23] found for Ge_{12}^{4+}.

In general the binding energies per atom are higher for the neutral clusters and decrease both in the negatively and positively charged species as expected. Notable is also the finding that the binding energies for the minima have only slightly lower values than those of the corresponding transition states.

Acknowledgment. We are indebted to the National Science Foundation for partial support of this work under Grants CHE-0209857 and CHE-0716718. Part of this work was undertaken with the financial support from CNCSIS-Roumania.

Supporting Information Available: Figures 1S−6S as cited in the text. This material is available free of charge via the Internet at http://pubs.acs.org.

References

(1) Wade, K. *Chem. Commun. (Cambridge)* **1971**, 792.

(2) Wade, K. *Adv. Inorg. Chem. Radiochem*. **1976**, *18*, 1.

(3) Mingos, D. M. P. *Nat. Phys. Sci*. **1972**, *99*, 236.

(4) Mingos, D. M. P. *Acc. Chem. Res*. **1984**, *17*, 311.

(5) Williams, R. E. *Chem. Rev*. **1992**, *92*, 177.

(6) King, R. B.; Rouvray, D. H. *J. Am. Chem. Soc*. **1977**, *99*, 7834.

(7) King, R. B. *Chem. Rev.* **1991**, *101*, 1119.

(8) Kasper, J. S.; Lucht, C. M.; Harker, D. *Acta Crystallogr*. **1950**, *3*, 436.

(9) Dustin, D. F.; Dunks, G. B.; Hawthorne, M. F. *J. Am. Chem. Soc.* **1973**, *95*, 1109.

(10) Eady, C. R.; Johnson, B. F. G.; Lewis, J.; Mason, R.; Hitchcock, P. B.; Thomas, K. M. *Chem. Commun. (Cambridge)* **1977**, 385.

(11) King, R. B. *Rev. Roum. Chim.* **2002**, *47*, 1005.

(12) Sevov, S. C.; Corbett, J. D. *Inorg. Chem.* **1991**, *30*, 4875.

(13) Zintl, E.; Goubeau, J.; Dullenkopf, W. *Z. Phys. Chem., Abt. A* **1931**, *154*, 1.

(14) Zintl, E.; Harder, A. *Z. Phys. Chem., Abt. A* **1931**, *154*, 47.

(15) Zintl, E.; Dullenkopf, W. *Z. Phys. Chem., Abt. B* **1932**, *16*, 183.

(16) Zintl, E.; Kaiser, H. *Z. Anorg. Allgem. Chem.* **1933**, *211*, 113.

(17) King, R. B. *Inorg. Chim. Acta* **1982**, *57*, 79.

(18) Ge_5, Ge_6, and Ge_7: King, R. B.; Silaghi-Dumitrescu, I.; Kun, A. *J. Chem. Soc., Dalton Trans.* **2002**, 3999.

(19) Ge_8: King, R. B.; Silaghi-Dumitrescu, I.; Lupan, A. *Dalton Trans.* **2005**, 1858.

(20) Ge_9: King, R. B.; Silaghi-Dumitrescu, I. *Inorg. Chem.* **2003**, *42*, 6701.

(21) Ge_{10}: King, R. B.; Silaghi-Dumitrescu, I.; Uţă, M. M. *Inorg. Chem.* **2006**, *45*, 4974.

(22) Ge_{11}: King, R. B.; Silaghi-Dumitrescu, I.; Lupan, A. *Inorg. Chem.* **2005**, *44*, 3579.

(23) Ge_{12}: King, R. B.; Silaghi-Dumitrescu, I.; Uţă, M. M. *Dalton Trans.* **2007**, 364.

(24) King, R. B.; Heine, T.; Corminboeuf, C.; Schleyer, P. v. R. *J. Am. Chem. Soc.* **2004**, *126*, 430.

(25) Chen, Z.; Neukemans, S.; Wang, X.; Janssens, E.; Zhou, Z.; Silverans, R. E.; King, R. B.; Schleyer, P. v. R.; Lievens, P. *J. Am. Chem. Soc.* **2006**, *128*, 12829.

(26) King, R. B.; Silaghi-Dumitrescu, I.; Lupan, A. *Chem. Phys.* **2006**, *327*, 344.

(27) Vosko, S. H.; Wilk, L.; Nusair, M. *Can. J. Phys*. **1980**, *58*, 1200.

(28) Lee, C.; Yang, W.; Parr, R. G. *Phys. Rev. B* **1988**, *37*, 785.

(29) Becke, A. D. *J. Chem. Phys.* **1993**, *98*, 5648.

(30) Stephens, P. J.; Devlin, F. J.; Chabalowski, C. F.; Frisch, M. J. *J. Phys. Chem.* **1994**, *98*, 11623.

(31) Frisch, M. J.; Trucks, G. W.; Schlegel, H. B.; Scuseria, G. E.; Robb, M. A.; Cheeseman, J. R.; Zakrzewski, V. G.; Montgomery, J. A., Jr.; Stratmann, R. E.; Burant, J. C.; Dapprich, S.; Millam, J. M.; Daniels, A. D.; Kudin, K. N.; Strain, M. C.; Farkas, O.; Tomasi, J.; Barone, V.; Cossi, M.; Cammi, R.; Mennucci, B.; Pomelli, C.; Adamo, C.; Clifford, S.; Ochterski, J.; Petersson, G. A.; Ayala, P. Y.; Cui, Q.; Morokuma, K.; Rega, N.; Salvador, P.; Dannenberg, J. J.; Malick, D. K.; Rabuck, A. D.; Raghavachari, K.; Foresman, J. B.; Cioslowski, J.; Ortiz, J. V.; Baboul, A. G.; Stefanov, B. B.; Liu, G.; Liashenko, A.; Piskorz, P.; Komaromi, I.; Gomperts, R.; Martin, R. L.; Fox, D. J.; Keith, T.; Al-Laham, M. A.; Peng, C. Y.; Nanayakkara, A.; Challacombe, M.; Gill, P. M. W.; Johnson, B.; Chen, W.; Wong, M. W.; Andres, J. L.; Gonzalez, C.; Head-Gordon, M.; Replogle, E. S.; Pople, J. A. *Gaussian 98, Revision A.11.3*; Gaussian, Inc.: Pittsburgh, PA, 2002.

(32) Archibong, E. F.; St-Amant, A. *J. Chem. Phys.* **1998**, *109*, 962.

(33) Xie, Y.; Schaefer, H. F.; King, R. B. *J. Am. Chem. Soc.* **2000**, *122*, 8746.

(34) Papas, B. N.; Schaefer, H. F. *J. Mol. Struct. THEOCHEM* **2006**, *768*, 175.

CT7002226